Crystal Structure of *Mycobacterium tuberculosis* Shikimate Kinase in Complex with Shikimic Acid and an ATP Analogue[†,‡]

Jianhua Gan,[§] Yijun Gu,[§] Yue Li,[||] Honggao Yan,[||] and Xinhua Ji*[,§]

Macromolecular Crystallography Laboratory, National Cancer Institute, Frederick, Maryland 21702, and Department of Biochemistry and Molecular Biology, Michigan State University, East Lansing, Michigan 48824

Received March 30, 2006; Revised Manuscript Received May 17, 2006

ABSTRACT: Shikimate kinase (SK) and other enzymes in the shikimate pathway are potential targets for developing nontoxic antimicrobial agents, herbicides, and antiparasite drugs, because the pathway is essential in microorganisms, plants, and parasites but absent from mammals. SK catalyzes the reaction of phosphoryl transfer from ATP to shikimic acid (SA). Since 2002, a total of 11 SK structures have been reported, but none contains either the two substrate (SA and ATP) or the two product (SA−phosphate and ADP) molecules. Here, we present three crystal structures of SK from *Mycobacterium tuberculosis* (MtSK), including apo-MtSK, a binary complex MtSK·SA, and the ternary complex of MtSK with SA and an ATP analogue, AMPPCP. The structures of apo-MtSK and MtSK·AMPPCP·SA make it possible to elucidate the conformational changes of MtSK upon the binding of both substrates; the structure of MtSK·AMPPCP·SA reveals interactions between the protein and γ-phosphate which indicate dynamic roles of catalytic residues Lys15 and Arg117.

Shikimate pathway is a biosynthetic pathway with many branches that leads to the synthesis of aromatic amino acids, folate cofactors, ubiquinone, and many secondary metabolites (*1*, *2*). The pathway is essential for algae, higher plants, bacteria, fungi, and parasite, whereas it is absent in mammals (*2*, *3*). Therefore, the pathway is a potential target for the development of nontoxic antimicrobial agents (*4*), herbicides (*5*), and antiparasite drugs (*6*).

Tuberculosis is a major threat to human health. According to the 1999 World Health Organization Report (*7*), *Mycobacterium tuberculosis* causes more deaths in adolescents and adults than any other single infection. The emergence of multidrug-resistant tuberculosis (>4% of new tuberculosis cases) has become a major challenge to the medical world. Shikimate kinase (SK,[1] EC 2.7.1.71), the fifth enzyme in the shikimate pathway, from *M. tuberculosis* (MtSK) is obviously an excellent target for developing novel anti-*M. tuberculosis* agents.

To date, a total of 11 crystal structures of SK have been reported, including four structures for MtSK [PDB accession codes 1L4U (*8*), 1L4Y (*8*), 1U8A (*9*), and 1WE2 (*10*)], three for *Erwinia chrysanthemi* SK [EcSK, PDB codes 1SHK (*11*), 2SHK (*11*), and 1E6C (*12*)], one for *Escherichia coli* SKI [EcolSKI, PDB code 1KAG (*13*)], one for *Campylobacter jejuni* SK [CjSK, PDB code 1V1A (*14*)], and two for *Helicobacter pylori* [HpSK, PDB codes 1ZUH and 1ZUI (*15*)]. These structures show that SK belongs to the family of nucleoside monophosphate (NMP) kinases, which are composed of three domains: the core, lid, and NMP-binding domains (*16*). The core domain contains a highly conserved P-loop, the lid domain closes over bound ATP and bears functionally essential residues, and the NMP-binding domain is responsible for recognizing and binding a specific NMP. NMP kinases undergo large domain movement upon substrate binding, for which adenylate kinase is the most extensively studied (*16*, *17*). The binding domain for shikimic acid (SA) in SK corresponds to the NMP-binding domain in NMP kinases.

SK catalyzes the transfer of a phosphoryl group from ATP to SA. The structural details of SK in complex with its substrate/product molecules will certainly provide valuable information for elucidating the mechanism of SK-catalyzed reaction and for structure-based drug design. Among the 11 previously reported structures, 1SHK (*11*), 1E6C (*12*), 1KAG (*13*), 1V1A (*14*), and 1ZUH (*15*) have neither SA nor a nucleotide bound in their active centers; 1L4U (*8*), 1L4Y (*8*), and 2SHK (*11*) are complexed with ADP only; 1ZUI (*15*) is complexed with SA only; and 1U8A (*9*) and 1WE2 (*10*) are complexed with both SA and ADP. Not available was a ternary structure that contains either the two substrates (SA and ATP) or the two products (SA−phosphate and

[†] This research was supported by NIH Grant GM51901 (to H.Y.) and the Intramural Research Program of the NIH, National Cancer Institute, Center for Cancer Research.

[‡] The coordinates and structure factors of apo-MtSK, MtSK·SA, and MtSK·AMPPCP·SA have been deposited with the Protein Data Bank (The Rutgers State University of New Jersey). The accession codes are 2G1J, 2G1K, and 1ZYU for apo-MtSK, MtSK·SA, and MtSK·AMPPCP·SA, respectively.

* To whom correspondence should be addressed. Phone: 301-846-5035. Fax: 301-846-6073. E-mail: jix@ncifcrf.gov.

[§] National Cancer Institute.

[||] Michigan State University.

[1] Abbreviations: NMP, nucleoside monophosphate; SA, shikimic acid; SK, shikimate kinase; MtSK, SK from *Mycobacterium tuberculosis*; EcSK, SK from *Erwinia chrysanthemi*; EcolSKI, SK I from *Escherichia coli*; CjSK, SK from *Campylobacter jejuni*; HpSK, SK from *Helicobacter pylori*; rmsd, root-mean-square deviation.

10.1021/bi0606290 CCC: $33.50
Published on Web 06/21/2006

ADP). Here, we present three crystal structures, including apo-MtSK, binary complex MtSK·SA, and the ternary complex of MtSK with SA and AMPPCP (an ATP analogue), which mimics the Michaelis complex for the MtSK-catalyzed phosphoryl transfer reaction.

EXPERIMENTAL PROCEDURES

Crystallization and Data Collection. The cloning, expression, and purification of MtSK have previously been reported (*18*). Single crystals were grown using the sitting-drop vapor diffusion method at 19 ± 1 °C. For apo-MtSK, the protein solution was composed of 9.3 mg/mL MtSK, 5 mM $MgCl_2$, and 0.25 M KCl in 50 mM Tris-HCl (pH 7.5). The well solution contained 0.2 M ammonium sulfate and 30% (w/v) poly(ethylene glycol) (PEG) monomethyl ether 5000 in 0.1 M MES (pH 6.5) buffer. The drops consisted of 0.2 μL of protein solution and 0.4 μL of well solution. For both MtSK·SA and MtSK·AMPPCP·SA crystals, the protein solution was composed of 9.3 mg/mL MtSK, 2.5 mM SA, 2.5 mM AMPPCP, 5.0 mM $MgCl_2$, and 0.25 M KCl in 50 mM Tris-HCl (pH 7.5). For MtSK·SA, the reservoir solution contained 2.0 M ammonium sulfate in 0.1 M sodium acetate (pH 4.5) buffer and the drop consisted of equal volumes of protein and well solutions. For MtSK·AMPPCP·SA, the reservoir solution contained 20% PEG 3000 in 0.1 N citrate (pH 5.5) buffer and the drop consisted of equal volumes of protein and well solutions. The crystals of apo-MtSK and MtSK·SA appeared within 1 week, whereas the crystals of MtSK·AMPPCP·SA appeared after 6 months.

The X-ray diffraction data were collected at the Southeast Regional Collaborative Access Team (SER-CAT) insertion device beamline 22-ID at the Advanced Photon Source (APS), Argonne National Laboratory. For the apo-MtSK and MtSK·AMPPCP·SA crystals, the cryoprotectant contained 20% glycerol and 80% well solution. The MtSK·SA crystal was protected by oil (type A; Hampton Research). The crystals were flash frozen with liquid nitrogen and kept at 100 K during data collection. The crystals diffracted to 2.0, 1.75, and 2.9 Å for apo-MtSK, MtSK·SA, and MtSK·AMPPCP·SA, respectively. The raw data were processed using DENZO and SCALEPACK packages (*19*). The X-ray data statistics are shown in Table 1.

Structure Solution and Refinement. The structures of apo-MtSK and MtSK·SA were solved with the molecular replacement program AMoRe (*20*) using the MtSK·MgADP binary complex structure [PDB entry 1L4Y (*8*)] as the search model after removing ADP, Mg^{2+}, water molecules, and polypeptide segments Asp34−Gly53 and Ala104−Arg130. The structure of MtSK·AMPPCP·SA was also solved with AMoRe (*20*) using the refined MtSK·SA structure as the search model after SA and solvent molecules were removed. The partial structures were subjected to rigid body refinement, simulated annealing, energy minimization, and grouped *B*-factor refinement followed by difference Fourier synthesis, which revealed the missing segments of the structure. Accordingly, the complete models were built. The apo-MtSK crystal was twinned with twinning law $h, -h - k, -l$. The twinning fraction was estimated to be 0.47 using the statistical method of Yeates (*21*), refined to 0.49, and fixed at 0.50 during the refinement.

The structure refinement was done with the program CNS (*22*) on a Silicon Graphics Fuel workstation. Bulk solvent correction was employed. During the refinement, the $2F_o - F_c$ and $F_o - F_c$ electron density maps were regularly calculated for inspecting and improving the model. Solvent molecules, as peaks $\geq 3\sigma$ on the $F_o - F_c$ electron density map with reasonable hydrogen bond networks, were included in the model at the later stage of the refinement and verified with omit maps. All graphics work was carried out using O (*23*). Illustrations were prepared with program packages MOLSCRIPT (*24*), BOBSCRIPT (*25*), RASTER3D (*26*), and PyMOL (Delano Scientific, LLC).

Table 1: X-ray Diffraction Data and Structure Refinement Statistics

	apo-MtSK	MtSK·SA	MtSK·AMPPCP·SA
resolution range (Å)	30.0−2.0	30.0−1.75	30.0−2.9
space group	$P3_1$	$P3_121$	$P3_121$
cell dimension			
$a = b$ (Å)	90.2	59.3	60.0
c (Å)	41.4	102.5	102.7
completeness (%), overall/last shell[a]	96.1/91.1	96.1/91.3	88.7/54.0
redundancy	2.7	3.5	4.1
$I/\sigma(I)$, overall/last shell	13.4/4.2	13.6/3.4	9.3/2.0
$R_{scaling}$,[b] overall/last shell	0.071/0.212	0.084/0.250	0.125/0.312
data for refinement	22558	20819	4488
data for *R*-free calcn	1121	1006	472
final *R*-factor[c]	0.175	0.222	0.196
final *R*-free	0.207	0.247	0.251
no. of amino acid residues	318	168	168
no. of water oxygen	231	174	48
no. of AMPPCP	0	0	1
no. of SA	0	1	1
rmsd			
bond distances (Å)	0.007	0.005	0.006
bond angles (deg)	2.0	1.2	1.1
Ramachandran plot			
most favored φ/ψ angles (%)	94.3	95.0	85.7
disallowed φ/ψ angles (%)	0	0	0

[a] The outmost shell of X-ray diffraction data for apo-MtSK, MtSK·SA, and MtSK·AMPPCP·SA is 2.07−2.0, 1.81−1.75, and 3.08−2.9 Å, respectively. [b] $R_{scaling} = \sum|I - \langle I\rangle|/\sum I$. [c] Crystallographic *R*-factor $= \sum_{hkl}||F_o| - |F_c||/\sum_{hkl}|F_o|$.

RESULTS AND DISCUSSION

Overall Structure. The refinement statistics for the three crystal structures can be found in Table 1. There are two MtSK molecules in the asymmetric unit of apo-MtSK, but one for the other two structures. The apo-MtSK structure contains 318 amino acid residues (two MtSK molecules, each containing residues Ala2−Gly113 and Ala121−Gln167), three SO_4^{2-} ions, and 231 water molecules; MtSK·SA contains residues Ala2−Gln169, three SO_4^{2-} ions, and 174 water molecules; and MtSK·AMPPCP·SA contains residues Ala2−Gln169, one AMPPCP, one SA, and 48 water molecules. The analysis of the structures using the validation program PROCHECK (*27*) reveals that more than 85% of the residues exhibit the most favored φ/ψ relationship and no residue has a disallowed φ/ψ relationship in the three structures (Table 1). The overall structure of MtSK·AMPPCP·SA is illustrated in Figure 1, where the $F_o - F_c$ electron density (annealed omit map) is shown for the AMPPCP and SA molecules. The core domain of MtSK is centered by a

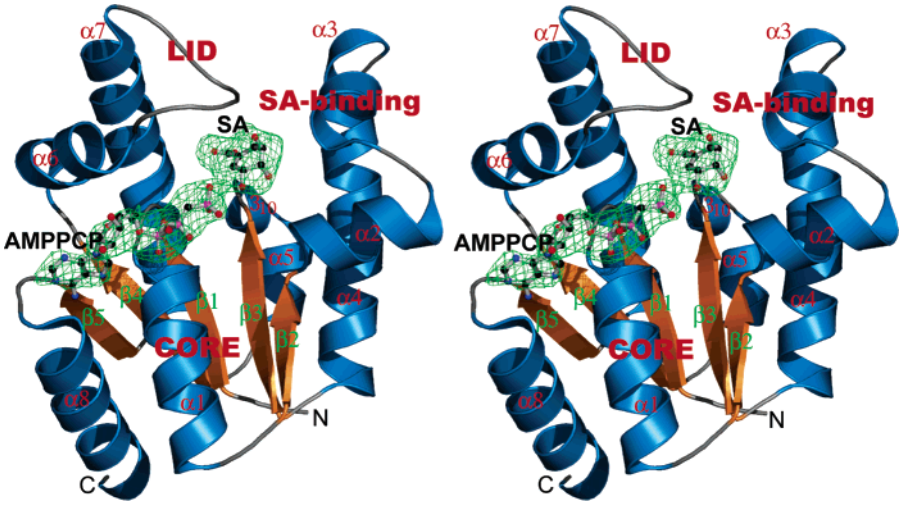

FIGURE 1: Stereoview showing the overall structure and representative electron density of the MtSK·AMPPCP·SA complex. Secondary structure elements are indicated by blue spirals for α-helices, yellow arrows for *β*-strands, and gray pipes for loops. The AMPPCP and SA molecules are shown as ball-and-stick models with atomic color scheme (C, black; N, blue; O, red; S, yellow; and P, pink). Electron density maps (annealed omit map, $F_o - F_c$, contoured at 3.0σ) are shown as green nets.

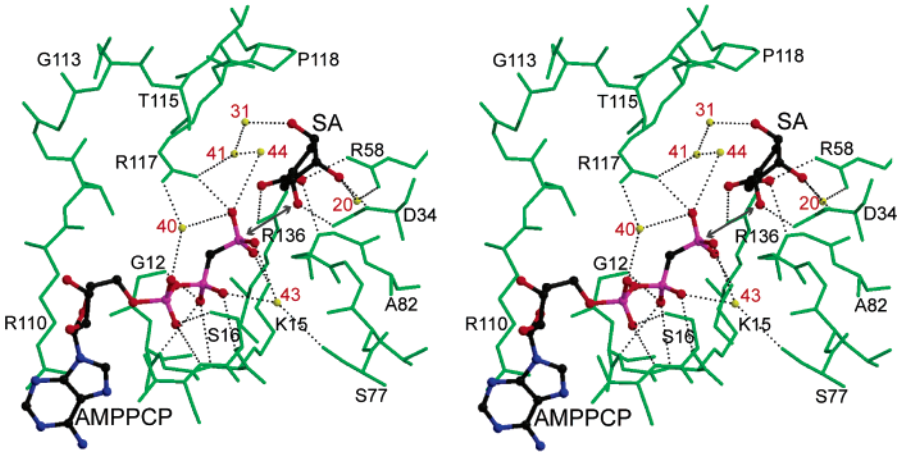

FIGURE 2: Stereoview showing the binding of AMPPCP and SA in MtSK·AMPPCP·SA. AMPPCP and SA are shown in atomic color (C, black; N, blue; O, red; and P, pink) as ball-and-stick models. Protein and water molecules are shown as green stick models and yellow spheres, respectively. The water molecules are labeled with numbers only. Hydrogen bonds are shown as dashed lines. The distance (4.1 Å) between the *γ*-phosphorus of bound AMPPCP and the 3-hydroxyl oxygen of SA is indicated with a double-headed arrow.

five-stranded parallel *β*-sheet; the lid domain contains residues 112−124; and the SA-binding domain contains α2, α3, and the N-terminal half of α4. The overall structure of MtSK·SA is similar to that of MtSK·AMPPCP·SA.

AMPPCP Binding. SK and many other nucleotide-binding enzymes contain a short conserved stretch of sequence GXXXXGKT/S, the P-loop (*28*), a giant anion hole that accommodates the *β*-phosphate of bound nucleotides. The interactions between MtSK and AMPPCP in the MtSK·AMPPCP·SA complex are illustrated in Figure 2 and compared with those found in the MtSK·MgADP (*8*) and MtSK·MgADP·SA(*10*) structures in Figure 3A. The *γ*-phosphate group interacts with the side chains of Lys15 and Arg117; the distance between the *γ*-phosphorus of AMPPCP and the 3-hydroxyl oxygen of SA is 4.1 Å (Figure 2). As previously observed, the binding of MgADP in the structures of MtSK·MgADP (*8*) and MtSK·MgADP·SA (*10*) is identical. The *β*-phosphate of AMPPCP mainly interacts with P-loop residues, Gly12, Gly14, Lys15, and Ser16, the α-phosphate of AMPPCP interacts with residues Ser16 and Thr17 (Figure 3A), and the adenine motiey of AMPPCP is sandwiched between Arg110 (Figure 2) and Pro155 (not shown). The structure of MtSK·AMPPCP·SA reveals interactions between the protein and *γ*-phosphate which reflect the dynamic roles of residues Lys15 and Arg117. In the two MgADP complexes, these two side chains interact with the *β*-phosphate, whereas in the AMPPCP complex, they interact with the *γ*-phosphate (Figure 3A). It is therefore obvious that these two side chains must be directly involved in the phosphoryl transfer reaction. MtSK has only two positively charged residues, Lys15 and Arg117, interacting with the substrate groups directly involved in the chemistry, in contrast to six positively charged residues in adenylate kinase and UMP/CMP kinase and five in guanylate kinase (*16*). There are three arginine residues from the lid domain of adenylate kinase or UMP/CMP kinase and two from the lid domain of guanylate kinase but only one from the lid domain of SK. Among the positively charged residues, only the lysine residue on the P-loop is conserved between SK and NMP kinases. Unfortunately, no Mg^{2+} ion is found in the MtSK·AMPPCP·SA structure. Residue Ser16, the only residue that is directly coordinated with the bound Mg^{2+} ion (*8*, *10*),

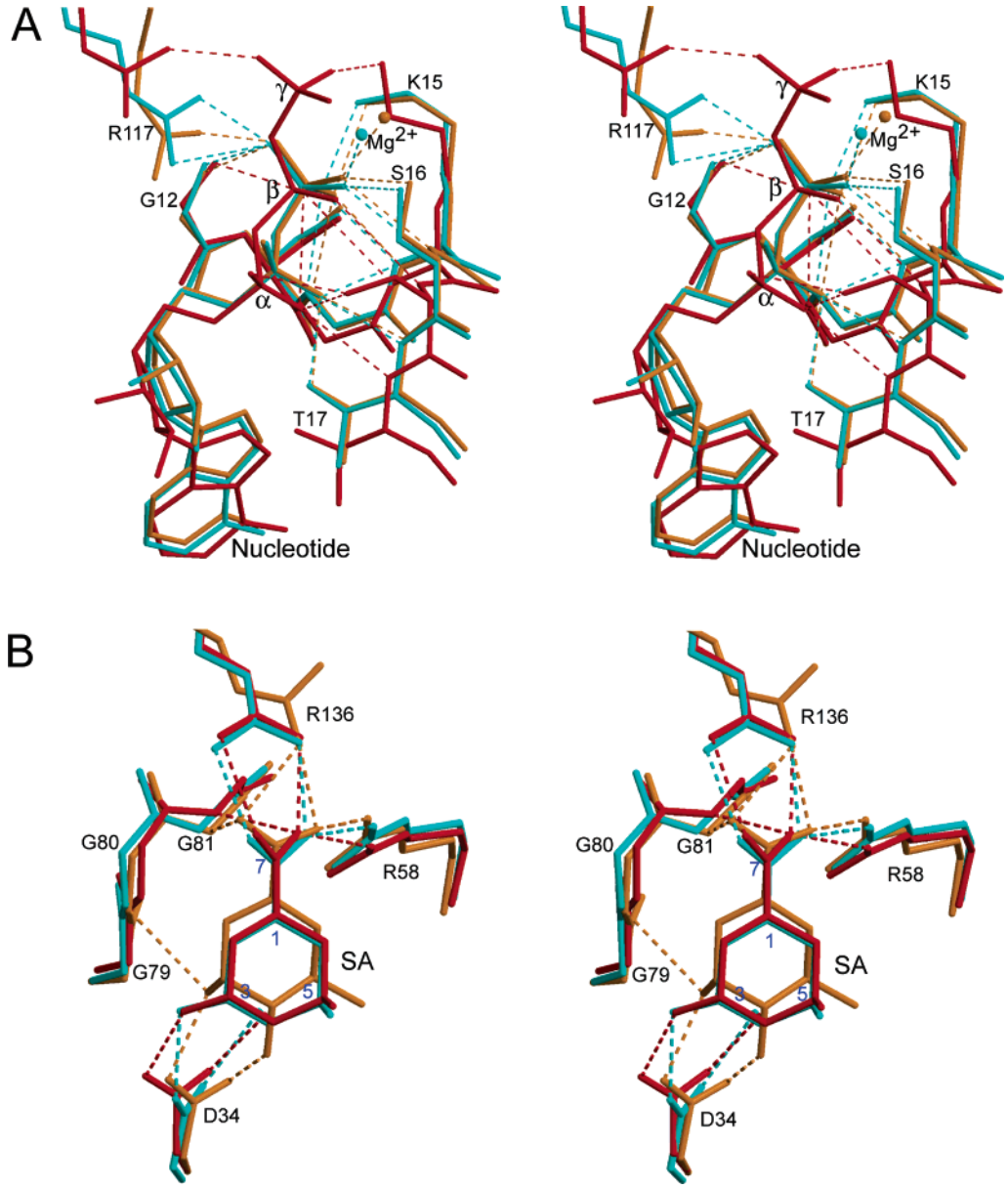

FIGURE 3: Stereoview showing the comparison of ligand binding in MtSK structures. (A) Alignment of bound nucleotide molecules in MtSK·AMPPCP·SA, MtSK·MgADP [PDB entry 1L4U (*8*)], and MtSK·MgADP·SA [PDB entry 1WE2 (*10*)] (shown as stick models in red, cyan, and orange, respectively). Hydrogen bonds between ligands and protein are shown as dashed lines. (B) Superposition of SA in the MtSK·AMPPCP·SA, MtSK·SA, and MtSK·MgADP·SA [PDB entry 1WE2 (*10*)] structures (shown as stick models in red, cyan, and orange, respectively). The hydrogen bonds between SA and protein are shown as dashed lines in the same color of the individual structure.

interacts with the nucleotide differently (Figures 3A and 4B). The details of Mg^{2+} coordination in the ternary substrate complex remain to be seen.

SA Binding. The SA-binding domain, residues 33−61, consists of helices α2 and α3 and the N-terminal region of helix α4 (Figure 1). The SA molecule is well defined in the MtSK·SA and MtSK·AMPPCP·SA structures (Figure 1). The interactions between the SA molecule and MtSK are shown in Figure 2. The SA-binding site is characterized by an SA-binding pocket with a number of charged residues that project into the cavity. The SA-binding pocket is formed by the hydrophobic residues of the SA-binding domain (Ile45, Phe49, and Phe57), the P-loop and three hydrophobic residues (Pro11, Pro118, and Leu119), and three highly conserved residues (Gly79, Gly80, and Gly81) (Figure 2). A number of charged residues project into the SA-binding pocket. The carboxylate group of SA interacts with the guanidium groups of Arg58 and Arg136; the carboxylate group of Asp34 forms H-bonds with the 3- and 4-hydroxyl groups of SA (Figure 2). The interactions between SA and SK were also observed in the structure of MtSK·MgADP·SA (*10*) with two exceptions. First, the guanidinium group of Arg136 interacts with only one of two oxygen atoms of the SA carboxyl group due to the flip of the guanidinium group. Second, an additional hydrogen bond is formed between the 3-hydroxyl group and the amide group of Gly80 (Figure 3B).

Conformational Changes of MtSK upon the Binding of Both Substrates. The lid domain of SK has high flexibility and undergoes extraordinary conformational changes upon substrate binding. It usually adopts "closed" conformation when the nucleoside triphosphate is bound in the active center to protect the bound triphosphate from being hydrolyzed (*17*). A comparison between an apo-EcSK structure (*12*) and the

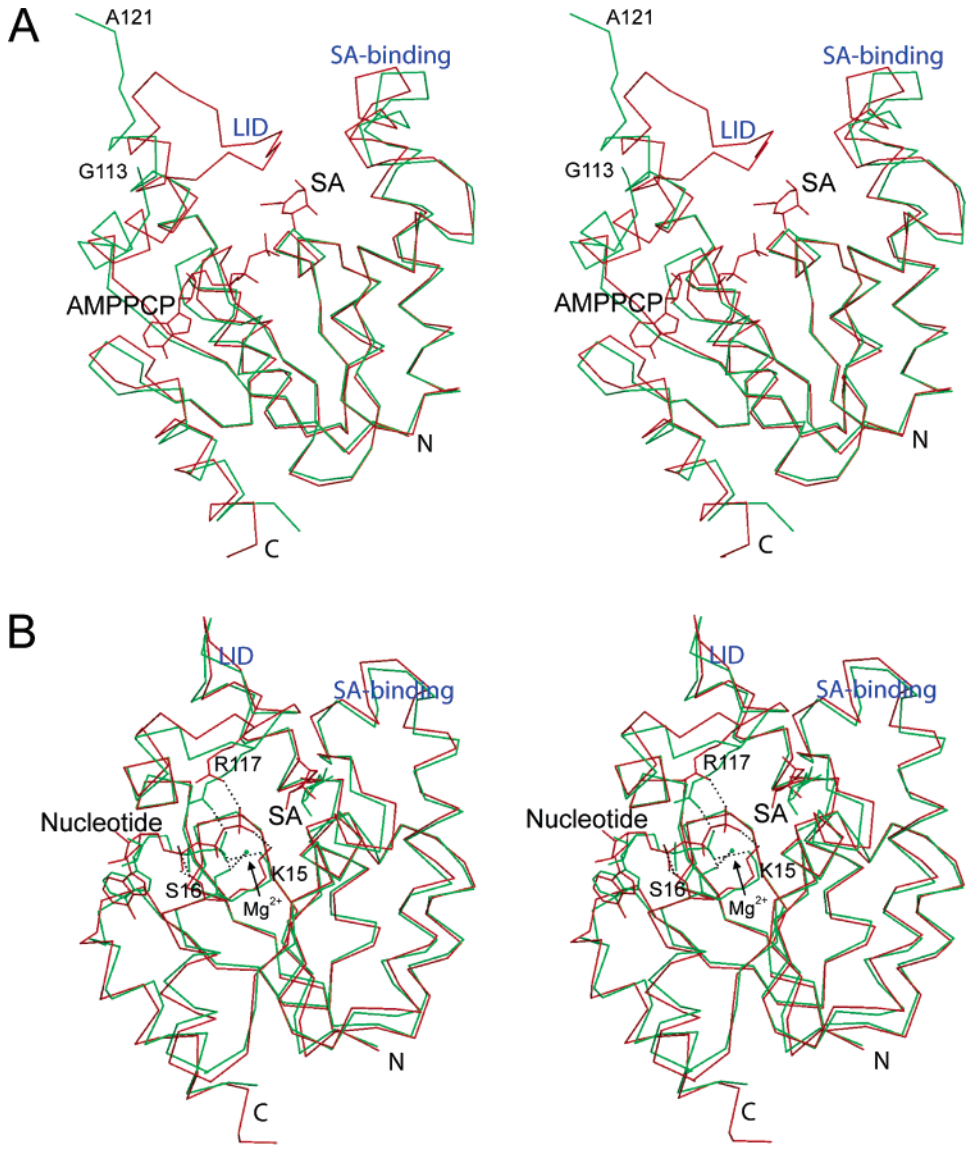

FIGURE 4: Stereoviews showing the conformational changes of the MtSK structure upon ligand binding. (A) The Cα trace alignment of MtSK·AMPPCP·SA and apo-MtSK (in red and green, respectively). The SA and AMPPCP molecules are shown as stick models. (B) The Cα trace alignment of MtSK·AMPPCP·SA and MtSK·MgADP·SA [PDB entry 1WE2 (*10*)] (in red and green, respectively). The nucleotides, SA, and the side chains of Lys15, Ser16, and Arg117 are shown as stick models. The Mg^{2+} ion is shown as a sphere. The interactions between nucleotides and the side chains of Arg117 and P-loop residues are highlighted with a dashed line in black.

MtSK·MgADP structure suggested that ADP binding induces a large hinged movement of the lid domain over the active site (*8*).

Previously, four MtSK structures were reported, including two structures for the binary complex MtSK·MgADP [PDB accession codes 1L4U and 1L4Y (*8*)] and the structures of two dead-end ternary complexes, MtSK·ADP·SA [PDB accession code 1U8A (*9*)] and MtSK·MgADP·SA [PDB accession code 1WE2 (*10*)]. In this study, we present three structures, including apo-MtSK, binary complex Mtsk·SA, and ternary complex MtSK·AMPPCP·SA. Comparison between structures of the same protein at various liganded states provides the opportunity to elucidate the conformational changes of MtSK upon ligand binding.

The alignment of apo-MtSK and MtSK·AMPPCP·SA is shown in Figure 4A. The protein conformation in the structure of MtSK·SA is virtually identical to that in MtSK·AMPPCP·SA with a root-mean-square deviation (rmsd) of 0.32 Å for all Cα positions, suggesting that SA binding defines the conformational change of the protein although it is not conclusive before the structure of MtSK in complex with an ATP (or ATP analogue) becomes available. The core domains of all three structures superimpose very well, but ligand binding induces significant movements of the other two domains.

The lid domain is the most flexible part of the protein. In apo-MtSK, the lid domain is wide open with seven residues (114−120) missing due to unobserved electron density (Figure 4A), indicating that the lid domain is highly flexible in the ligand-free form of the protein. When SA is bound, the lid domain is ordered and closed over onto the bound SA, as observed in the structures of both MtSK·SA and MtSK·AMPPCP·SA (Figures 1 and 4A). In addition, the SA-binding domain and the P-loop move closer to the core domain by ∼2 Å (Figure 4A).

The SO_4^{2-} Ion Inhibits the Binding of AMPPCP. The crystals of MtSK·SA and MtSK·AMPPCP·SA grew from the same protein solution but with different precipitants. With

PEG 3000, the MtSK·AMPPCP·SA complex was obtained; with ammonium sulfate, however, AMPPCP was not bound. Instead, a SO_4^{2-} ion was found in the P-loop. It interacts with the amide groups of Gly12, Ser13, Gly14, Lys15, and Ser16, forming hydrogen bonds within the distance of 2.8−3.0 Å. It also interacts with atom NZ of Lys15 directly and with the guanidinium group of Arg117 via bridging water molecules (not shown).

Similarly, a sulfate ion was found in the P-loop of the apo-MtSK structure, the crystals of which were grown from ammonium sulfate as well. In the previously reported structure of EcSK [PDB code 1E6C (*12*)] and HpSK [PDB code 1ZUI (*15*)], a PO_4^{3-} ion was found in the P-loop. It appears that negatively charged ions with a tetrahedral geometry, such as SO_4^{2-} and PO_4^{3-}, can inhibit SK from binding nucleotides bearing a β-phosphate. Thus, the structural basis has been provided for the effects of SO_4^{2-} on the function and conformational stability of SK reported previously (*29*).

Implications for the Mechanism of MtSK-Catalyzed Phosphoryl Transfer. The crystal structure of MtSK·AMPPCP·SA contains both SA and an ATP analogue. The difference between ATP and AMPPCP is the substitution of the oxygen that links the β- and γ-phosphates in ATP with a methylene group. It appears that the methylene substitution has minimal effects on the conformation of the triphosphate because the α- and β-phosphates of the two nucleotides superimpose well and the Pβ−C−Pγ angle (128.9°) is very similar to that of the nominal P−O−P angle (133.1°) (*30*). The distance between the γ-phosphorus of AMPPCP and the 3-hydroxyl oxygen of SA is 4.1 Å. However, this distance will most likely change when the Mg^{2+} ion is present inasmuch as both the nucleotide and the SA molecules shift significantly in the absence of Mg^{2+} (Figure 4B). Therefore, the information is not yet sufficient for the elucidatation of the associative (S_N2-like) or dissociative (S_N1-like) character of the transition state of MtSK-catalyzed phosphoryl transfer reaction in terms of the degree of bond cleavage between the $\beta-\gamma$ bridging oxygen and the γ-phosphorus and bond formation between the γ-phosphorus and the incoming nucleophile.

The primary candidates for the transition state stabilization are the guanidinium group of Arg117 and the ammonium group of Lys15 (Figure 2). The positions of the guanidinium and the ammonium groups at the transition state may be inferred or delimited from their positions in the ternary enzyme−substrate complex and in the ternary enzyme−product complex. The structure of MtSK·AMPPCP·SA mimics that of the ternary enzyme−substrate complex, while the structure of the ternary enzyme−product complex or its mimic remains to be determined. Although the stabilization of the transition state by Arg117 and Lys15 may be a major component of MtSK catalysis, Asp34 also facilitates the reaction by forming a hydrogen bond to the 3-hydroxyl group of SA (Figure 2) and thereby increasing the nucleophilicity of the 3-hydroxyl oxygen. It may also act as a general base by accepting the proton from the 3-hydroxyl group of SA, although this is unlikely to be a rate-limiting step in the reaction.

ACKNOWLEDGMENT

We thank Drs. John J. Chrzas and Zhongmin Jin for help during data collection. X-ray diffraction data were collected at the SER-CAT 22-ID beamline of the APS, Argonne National Laboratory. Supporting institutions may be found at www.ser-cat.org/members.html.

REFERENCES

1. Bentley, R. (1990) The shikimate pathway—a metabolic tree with many branches, *Crit. Rev. Biochem. Mol. Biol. 25*, 307−384.
2. Haslam, E. (1993) *Shikimic Acid: Metabolism and Metabolites*, John Wiley & Sons, Chichester.
3. Kishore, G. M., and Shah, D. M. (1988) Amino acid biosynthesis inhibitors as herbicides, *Annu. Rev. Biochem. 57*, 627−663.
4. Davies, G. M., Barrett-Bee, K. J., Jude, D. A., Lehan, M., Nichols, W. W., Pinder, P. E., Thain, J. L., Watkins, W. J., and Wilson, R. G. (1994) (6*S*)-6-fluoroshikimic acid, an antibacterial agent acting on the aromatic biosynthetic pathway, *Antimicrob. Agents Chemother. 38*, 403−406.
5. Coggins, J. R. (1989) The shikimate pathway as a target for herbicides, in *Herbicides and Plant Metabolism* (Dodge, A., Ed.) pp 97−112, Cambridge University Press, Cambridge, U.K.
6. Ridley, R. G. (1998) Planting new targets for antiparasitic drugs, *Nat. Med. 4*, 894−895.
7. World Health Organization (1999) Report on infectious diseases: Removing obstacles to healthy development, World Health Organization, Geneva.
8. Gu, Y., Reshetnikova, L., Li, Y., Wu, Y., Yan, H., Singh, S., and Ji, X. (2002) Crystal structure of shikimate kinase from *Mycobacterium tuberculosis* reveals the dynamic role of the LID domain in catalysis, *J. Mol. Biol. 319*, 779−789.
9. Dhaliwal, B., Nichols, C. E., Ren, J., Lockyer, M., Charles, I., Hawkins, A. R., and Stammers, D. K. (2004) Crystallographic studies of shikimate binding and induced conformational changes in *Mycobacterium tuberculosis* shikimate kinase, *FEBS Lett. 574*, 49−54.
10. Pereira, J. H., de Oliveira, J. S., Canduri, F., Dias, M. V., Palma, M. S., Basso, L. A., Santos, D. S., and de Azevedo, W. F., Jr. (2004) Structure of shikimate kinase from *Mycobacterium tuberculosis* reveals the binding of shikimic acid, *Acta Crystallogr. D 60*, 2310−2319.
11. Krell, T., Coggins, J. R., and Lapthorn, A. J. (1998) The three-dimensional structure of shikimate kinase, *J. Mol. Biol. 278*, 983−997.
12. Krell, T., Maclean, J., Boam, D. J., Cooper, A., Resmini, M., Brocklehurst, K., Kelly, S. M., Price, N. C., Lapthorn, A. J., and Coggins, J. R. (2001) Biochemical and X-ray crystallographic studies on shikimate kinase: The important structural role of the P-loop lysine, *Protein Sci. 10*, 1137−1149.
13. Romanowski, M. J., and Burley, S. K. (2002) Crystal structure of the *Escherichia coli* shikimate kinase I (AroK) that confers sensitivity to mecillinam, *Proteins: Struct., Funct., Genet. 47*, 558−562.
14. Badger, J., Sauder, J. M., Adams, J. M., Antonysamy, S., Bain, K., Bergseid, M. G., Buchanan, S. G., Buchanan, M. D., Batiyenko, Y., Christopher, J. A., Emtage, S., Eroshkina, A., Feil, I., Furlong, E. B., Gajiwala, K. S., Gao, X., He, D., Hendle, J., Huber, A., Hoda, K., Kearins, P., Kissinger, C., Laubert, B., Lewis, H. A., Lin, J., Loomis, K., Lorimer, D., Louie, G., Maletic, M., Marsh, C. D., Miller, I., Molinari, J., Muller-Dieckmann, H. J., Newman, J. M., Noland, B. W., Pagarigan, B., Park, F., Peat, T. S., Post, K. W., Radojicic, S., Ramos, A., Romero, R., Rutter, M. E., Sanderson, W. E., Schwinn, K. D., Tresser, J., Winhoven, J., Wright, T. A., Wu, L., Xu, J., and Harris, T. J. (2005) Structural analysis of a set of proteins resulting from a bacterial genomics project, *Proteins: Struct., Funct., Genet. 60*, 787−796.
15. Cheng, W. C., Chang, Y. N., and Wang, W. C. (2005) Structural basis for shikimate-binding specificity of *Helicobacter pylori* shikimate kinase, *J. Bacteriol. 187*, 8156−8163.
16. Yan, H., and Ysai, M.-D. (1999) Nucleoside monophosphate kinases: structure, mechanism, and substrate specificity, *Adv. Enzymol. Relat. Areas Mol. Biol. 73*, 103−134.
17. Vonrhein, C., Schlauderer, G. J., and Schulz, G. E. (1995) Movie of the structural changes during a catalytic cycle of nucleoside monophosphate kinases, *Structure 3*, 483−490.
18. Gu, Y., Reshetnikova, L., Li, Y., Yan, H., Singh, S. V., and Ji, X. (2001) Crystallization and preliminary X-ray diffraction analysis

of shikimate kinase from *Mycobacterium tuberculosis* in complex with MgADP, *Acta Crystallogr. D 57*, 1870−1871.
19. Otwinowski, Z., and Minor, W. (1997) Processing of X-ray diffraction data collected in oscillation mode, *Methods Enzymol. 276*, 307−326.
20. Navaza, J. (1994) An automated package for molecular replacement, *Acta Crystallogr. A 50*, 157−163.
21. Yeates, T. O. (1997) Detecting and overcoming crystal twinning, *Methods Enzymol. 276*, 344−358.
22. Brünger, A. T., Adams, P. D., Clore, G. M., DeLano, W. L., Gros, P., Grosse-Kunstleve, R. W., Jiang, J. S., Kuszewski, J., Nilges, M., Pannu, N. S., Read, R. J., Rice, L. M., Simonson, T., and Warren, G. L. (1998) Crystallography & NMR system: A new software suite for macromolecular structure determination, *Acta Crystallogr. D 54*, 905−921.
23. Jones, T. A., and Kjeldgaard, M. (1997) Electron-density map interpretation, *Methods Enzymol. 277*, 173−208.
24. Kraulis, P. J. (1991) MOLSCRIPT: a program to produce both detailed and schematic plots of protein structures, *J. Appl. Crystallogr. 24*, 946−950.
25. Esnouf, R. M. (1997) An extensively modified version of MolScript that includes greatly enhanced coloring capabilities, *J. Mol. Graphics Modell. 15*, 132−134.
26. Merritt, E. A., and Bacon, D. J. (1997) Raster3D: photorealistic molecular graphics, *Methods Enzymol. 277*, 505−524.
27. Laskowski, R. A., MacArthur, M. W., Moss, D. S., and Thornton, J. M. (1993) PROCHECK: a program to check stereochemical quality of protein structures, *J. Appl. Crystallogr. 26*, 283−291.
28. Walker, J. E., Saraste, M., Runswick, M. J., and Gay, N. J. (1982) Distantly related sequences in the alpha- and beta-subunits of ATP synthase, myosin, kinases and other ATP-requiring enzymes and a common nucleotide binding fold, *EMBO J. 1*, 945−951.
29. Cerasoli, E., Kelly, S. M., Coggins, J. R., Lapthorn, A. J., Clarke, D. T., and Price, N. C. (2003) Effects of salts on the function and conformational stability of shikimate kinase, *Biochim. Biophys. Acta 1648*, 43−54.
30. Yount, R. G. (1975) ATP analogs, *Adv. Enzymol. Relat. Areas Mol. Biol. 43*, 1−56.

BI0606290